A New Quick Response and High Efficiency Control Strategy of an Induction Motor

ISAO TAKAHASHI TOSHIHIKO NOGUCHI
Technological University of Nagaoka
1603-1 Kamitomioka Nagaoka Japan, Zip 949-54

Abstract -- New quick response and high efficiency control of an induction motor which is quite different from that of field oriented one is proposed. The most obvious difference between the two are as follows;
(1) The proposed scheme is based on limit cycle control of both flux and torque using optimum PWM output voltage. An switching table is employed for selecting the optimum inverter output voltage vectors so as to attain as fast torque response, low inverter switching frequency and low harmonic losses as possible.
(2) The efficiency optimization in the steady state operation is also considered. It can be achieved by controlling the amplitude of the flux in accordance with the torque command.
To verify the feasibility of this scheme, experiment, simulation and comparison with field oriented control are carried out. The results prove the excellent characteristics for torque response and efficiency, which confirm the validity of this control scheme.

I. INTRODUCTION

According to the advance of factory automation, servo systems became indispensable to various applications such as industrial robots and numerical controlled machinery. Especially, the progress of an ac servo system is remarkable owing to maintenance free system. In recent years, it becomes to employ field oriented control, which enables an induction motor to attain as quick torque response as a dc motor. The principle of its torque generation is based on the interaction between the flux and current like a dc motor [1] . Fig.1(a) is a system configuration of a typical field orientation drive. In this system, the flux current component I_0* and the torque current component I_T* are estimated from both flux command ψ_2* and torque command T* by using a calculator possessing motor parameters. The system usually employs a position sensor for coordinate transformation of the current components and a current controlled inverter. Therefore, if the values used in the calculator deviate from the correct ones, both steady state and transient response would be degraded. A number of papers have reported the problem and explored the means of compensation [2] - [4] . There also remains some problems concerning instantaneous current control. Since the current controlled inverter contains three independent hysteresis comparators, it is difficult to avoid increase of the inverter switching frequency, torque ripple and harmonic losses of the machine in the steady state operation. Moreover, when the PWM inverter saturates, sufficient torque response would not be expected.

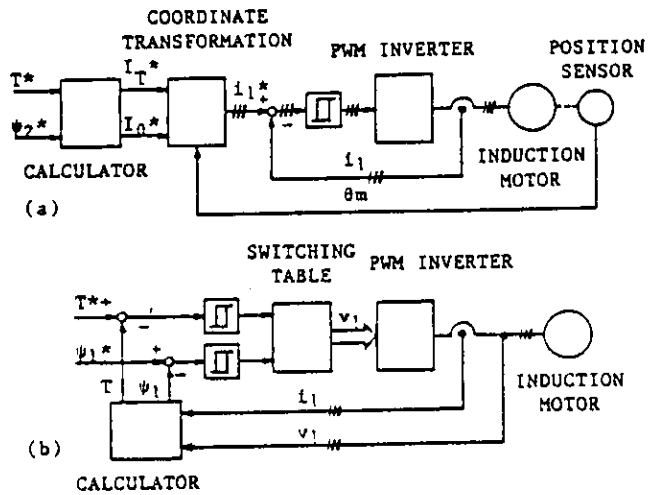

Fig.1. Comparison between two schemes
(a) Field oriented control
(b) Newly proposed scheme

This paper describes a novel control scheme of an induction motor [5]. The principle of it is based on limit cycle control and it makes possible both quick torque response and high efficiency operation at the same time. Fig.1(b) shows a system configuration of the proposed scheme. In this system, the instantaneous values of the flux and torque are calculated from only the primary variables. They can be controlled directly and independently by selecting optimum inverter switching modes. The selection is made so as to restrict the errors of the flux and torque within the hysteresis bands and to obtain the fastest torque response and highest efficiency at every instant. It enables both quick torque response in the transient operation, and reduction of the harmonic losses and acoustic noise. Moreover, the implementation of an efficiency controller is also considered in oder to improve the efficiency in the steady state operation.

II. DYNAMIC BEHAVIOR OF AN INDUCTION MOTOR

By using instantaneous vectors, the behavior of a machine can be conveniently expressed not only in the steady state but also in the transient state. In this section, in oder to examine the transient torque response of an induction motor, an application of the vectors to the characteristic equations is described.

The primary voltage vector v_1 is defined by the following expression [6].

$$v_1=\sqrt{2/3}\{v_{1a}+v_{1b}\exp(j2\pi/3)+v_{1c}\exp(j4\pi/3)\} \quad (1)$$

where v_{1a}, v_{1b} and v_{1c} are instantaneous values of the primary line-to-neutral voltages. Similarly, the primary current vector i_1 and the secondary current vector i_2 are given by

$$i_1=\sqrt{2/3}\{i_{1a}+i_{1b}\exp(j2\pi/3)+i_{1c}\exp(j4\pi/3)\} \quad (2)$$

$$i_2=\sqrt{2/3}\{i_{2a}+i_{2b}\exp(j2\pi/3)+i_{2c}\exp(j4\pi/3)\} \quad (3)$$

These vectors are represented in a d-q stationary reference frame. Using the vector notation, the equations of a two pole induction motor can be written as

$$\begin{bmatrix} v_1 \\ 0 \end{bmatrix} = \begin{bmatrix} R_1+pL_{11} & pM \\ (p-j\dot{\theta}m)M & R_2+(p-j\dot{\theta}m)L_{22} \end{bmatrix} \begin{bmatrix} i_1 \\ i_2 \end{bmatrix} \quad (4)$$

CH2207-9/85/0000-0496$01.00 © 1985 IEEE

IAS85:21D

$$T=\psi_1\cdot(-ji_1) \tag{5}$$

where R_1 : stator resistance, R_2 : rotor resistance, L_{11} : stator self inductance, L_{22} : rotor self inductance, M : mutual inductance, θ_m : mechanical angular velocity, T : electromagnetic torque, $\cdot$: scalar product and ψ_1 : primary flux linkage vector.
ψ_1 is given by

$$\psi_1=L_{11}i_1+Mi_2 \tag{6}$$

Under the condition of a constant amplitude of ψ_1, i.e. a constant amplitude of the magnetizing current vector i_0 of the stator, let's examine the torque step response of the motor. i_0 is obtained by dividing Eq.(6) by L_{11}.

$$i_0=\psi_1/L_{11}=i_1+(M/L_{11})i_2 \tag{7}$$

Both i_0 and i_1 can be written in the form of the polar coordinates as

$$i_0=I_0\exp(j\theta_0),\quad i_1=I_1\exp(j\theta_0) \tag{8}$$

where I_0 is considered to be a constant reference vector and θ_0 is an angle between i_0 and the d-axis. Substituting Eq.(8) into Eqs.(4) and (7), the following relation can be obtained from the rotor equation in Eq.(4).

$$I_1=\frac{R_2+(p+j\dot\theta s)L_{22}}{R_2+(p+j\dot\theta s)\ell}I_0 \tag{9}$$

where $\ell=(L_{11}L_{22}-M^2)/L_{11}$ and $\dot\theta s=\dot\theta_0-\dot\theta m$. $\dot\theta s$ is an instantaneous slip angular frequency of ψ_1 referred to the rotor. Assuming the condition of constant $\dot\theta m$, if the step change of $\dot\theta_0$ is applied at $t=0$, $\dot\theta s$ can be also regarded to be stepwise at $t=0$ and then constant.

Substituting Eqs.(7) and (8) into Eq.(5), the torque is represented by using I_0 and I_1.

$$T=L_{11}I_0\mathcal{L}^{-1}\{\mathrm{Im}[I_1(s)]\} \tag{10}$$

where $\mathcal{L}^{-1}$ means the inverse Laplace transformation and Im means the imaginary part of the vectors. Consequently, by substituting the Laplace transformed I_1 of Eq.(9) into Eq.(10), the solution can be derived as

$$\begin{aligned}T=&\frac{\dot\theta sR_2M^2I_0^2}{z^2}-\left(\frac{R_2M^2I_0^2}{\ell z}\sin(\dot\theta st+\alpha)\right.\\&-\frac{L_{11}I_0}{\ell}[L_{22}I_0-\ell\mathrm{Re}(I_1|_{t=0})]\sin\dot\theta st\\&\left.-L_{11}I_0\mathrm{Im}(I_1|_{t=0})\cos\dot\theta st\right)\exp(-R_2t/\ell)\end{aligned} \tag{11}$$

where $z=\{R_2^2+(\dot\theta s\ell)^2\}^{1/2}$, $\alpha=\tan^{-1}(\dot\theta s\ell/R_2)$ and Re means the real part of the vectors. This equation represents the torque step response to the step change of $\dot\theta s$ under a constant $|\psi_1|$. The first and second terms of Eq.(11) show steady state and transient torque respectively.

By differentiating Eq.(11) with respect to t, the rate of increasing torque at t=0 can be obtained.

$$\left.\frac{dT}{dt}\right|_{t=0}=\frac{L_{11}I_0}{\ell}\{[L_{22}I_0-\ell\mathrm{Re}(I_1|_{t=0})]\dot\theta s-R_2\mathrm{Im}(I_1|_{t=0})\} \tag{12}$$

Since the coefficient of $\dot\theta s$ is always positive and large, the quick torque response can be attained by using as much $\dot\theta s$ as possible. Fig.2 shows some simulation results of the torque response to the step change of $\dot\theta s$. The rate increase is approximately propotional to $\dot\theta s$, but the torque has the maximum value at $\dot\theta s=2\pi\cdot15$ rad/sec in the steady state.

III. SPACIAL FLUX VECTOR CONTROL BY PWM INVERTER

In the preceding section, an ideal power source with sinusoidal voltage and variable frequency output was considered. In practice, a power source which has inherently stepwise voltage waveforms such as a PWM inverter should be considered. The instantaneous vectors of the PWM inverter are regarded as discrete values, and the analysis using the instantaneous vectors is suitable for investigating dynamic behavior of the machine.

Fig.3 shows a schematic diagram of a PWM inverter drive system. In this figure, the line-to-neutral voltage v_{1a}, v_{1b} and v_{1c} are determined only by the inverter switching modes. Considering the combinations of the status of switches Sa, Sb and Sc, the inverter has eight conduction modes. By using switching functions Sa, Sb and Sc of which value is either 1 or 0, the primary voltage vector v_1 of Eq.(1) is represented as

$$v_1(Sa,Sb,Sc)=\sqrt{2/3}V[Sa+Sb\exp(j2\pi/3)+Sc\exp(j4\pi/3)] \tag{13}$$

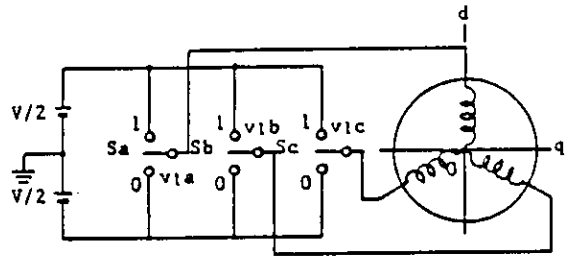

Fig.3. Schematic diagram of PWM inverter

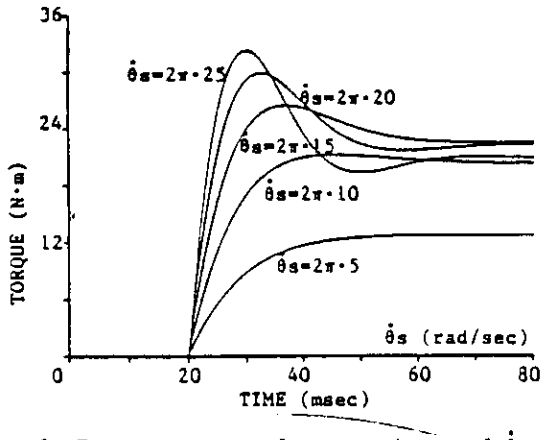

Fig.2. Torque response for step change of $\dot\theta s$

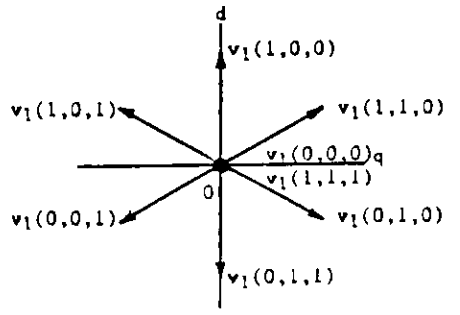

Fig.4. Instantaneous voltage vectors

where V is a dc link voltage of the PWM inveter. According to the combination of the switching modes, the voltage vectors are specified for eight kinds of vectors, two of which are zero voltage vectors $v_1(0,0,0)$ and $v_1(1,1,1)$, and the others are nonzero voltage vectors $v_1(0,0,1)$, $\cdots$, $v_1(1,1,0)$ as shown in Fig.4 [6] - [8].

Since the flux linkage vector is expressed by an integral of the voltage vector, substituting Eq.(6) into the stator equation in Eq.(4), the primary flux linkage vector ψ_1 is represented as a different style as follows.

$$\psi_1=\int(v_1-R_1 i_1)dt \tag{14}$$

During the switching intervals, each vector $v_1(0,0,0)$, $\cdots$, $v_1(1,1,1)$ is constant so that substituting Eq.(13) into Eq.(14) gives

$$\psi_1=\sqrt{2/3}\,V[Sa+Sb\exp(j2\pi/3)+Sc\exp(j4\pi/3)]t - R_1\int i_1 dt+\psi_1|_{t=0} \tag{15}$$

Considering that the voltage drop of the winding is small, the trajectry of ψ_1 moves in direction to the inverter output voltage vecter [7] - [9]. When the output is one of the nonzero voltage vectors, ψ_1 moves at a constant velocity which is propotional to the output voltage. In the case of a zero voltage vector, the velocity is very small and considered to be approximately zero because of the small value of $R_1 i_1$. Therefore, by selecting these vectors appropriately, the trajectry of ψ_1 can follow up to the specified locus. For example, by selecting adequate voltage vectors, $|\psi_1|$ can be kept constant as illustlated in Fig.5 and the rotating velocity of ψ_1 can be controlled by changing the output ratio between zero vectors and the others.

Thus $\dot{\theta}s$ and $|\psi_1|$ is greatly concerned with the dynamic torque and efficiency. If the amplitude and rotating velocity of ψ_1 can be changed freely, the desirable torque control and minimum loss operation would be obtained at a time.

IV. TORQUE CONTROL FOR QUICK RESPONSE

Fig.5 shows an example of constant $|\psi_1|$ control. The selection of $v_1(Sa,Sb,Sc)$ is made so that the error between $|\psi_1|$ and its command $|\psi_1|^*$ satisfies to be within the limits of $\Delta|\psi_1|$, i.e.

$$|\psi_1|^*-\Delta|\psi_1|/2 \le |\psi_1| \le |\psi_1|^*+\Delta|\psi_1|/2 \tag{16}$$

The selection depends on not only the error of the amplitude but also the direction of ψ_1. As shown in Fig.5, the inverter output voltage vectors change periodically by $\pi/3$ rad steps. Accordingly, in order to discriminate the direction, the d-q plane is devided into six regions as

$$(2N-3)\pi/6 \le \theta(N) \le (2N-1)\pi/6 \tag{17}$$

where N=1, $\cdots$,6. For example, if ψ_1 is in the region of $\theta(2)$, $v_1(0,1,0)$ and $v_1(0,1,1)$ can satisfy Eq.(16) for clockwise rotation. When $|\psi_1|$ reaches the upper limit of $|\psi_1|^*+\Delta|\psi_1|/2$, $v_1(0,1,1)$ must be selected. When $|\psi_1|$ reaches the lower limit of $|\psi_1|^*-\Delta|\psi_1|/2$, $v_1(0,1,0)$ must be selected. On the other hand, for counterclockwise rotation, $v_1(1,0,0)$ and $v_1(1,0,1)$ should be selected in $\theta(2)$. Thus, two dimensional limit cycle control of ψ_1 makes possible a constant $|\psi_1|$ by selecting the appropriate voltage vectors.

According to Eq.(12), under constant $|\psi_1|$ control, the rate of increasing torque is almost propotional to $\dot{\theta}s$. Therefore, when T is small comparing with its command T*, it is necessary to increase T as fast as possible by applying the fastest $\dot{\theta}_0$. Accelerating vectors which possess the maximum $\dot{\theta}_0$ of clockwise direction can be uniquely selected by the regions $\theta(N)$. When T reaches T*, it is better to decrease T as slowly as possible for decreasing the inverter switching frequency. The slowest degenerative operation might be obtained by using zero voltage vectors. Fig.6 shows torque control of this scheme for the clockwise operation. The selection of $v_1(Sa,Sb,Sc)$ is made so that the error of T satisfies to be within the limits of both ΔT and $\Delta|\psi_1|$, i.e.

$$T^*-\Delta T \le T \le T^* \quad (\text{when } \psi_1 \text{ rotates clockwise})$$
$$T^* \le T \le T^*+\Delta T \quad (\text{when } \psi_1 \text{ rotates counterclockwise}) \tag{18}$$

Assuming that ψ_1 rotates clockwise, when T reaches T*, a zero voltage vector is selected to stop ψ_1 and degenerate T. This corresponds to the case of $\dot{\theta}s=-\dot{\theta}m<0$ in Eq.(12). On the other hand, when T reaches $T^*-\Delta T$, one of the accelerating vectors which rotates ψ_1 clockwise at maximum angular velocity is selected. For counterclockwise rotation, the zero and one of the accelerating voltage vectors which rotate ψ_1 counterclockwise as much velocity are alternately selected to satisfiy $T^* \le T \le T^*+\Delta T$.

As shown in Fig.7, the status of the errors of $|\psi_1|$ and T can be detected and digitalized by simple two and three level hysteresis comparators. The contents of the optimum switching table, as stated before, is determined only by the errors and region $\theta(N)$. Accordingly, accessing the table, in which the inverter output voltage vectors are listed, by the comparator outputs and $\theta(N)$ signals, the optimum switching pattern desirable for drive can directly obtained. In this figure, ϕ and τ are digitalized outputs of the errors, and the signals of the $\theta(N)$ are generated by comparing d and q-axis components of the flux linkage vector with its amplitude. The switching table is referred by the outputs of the comparators ϕ, τ and $\theta(N)$. A combination of them defines only an inverter output voltage vector $v_1(Sa,Sb,Sc)$.

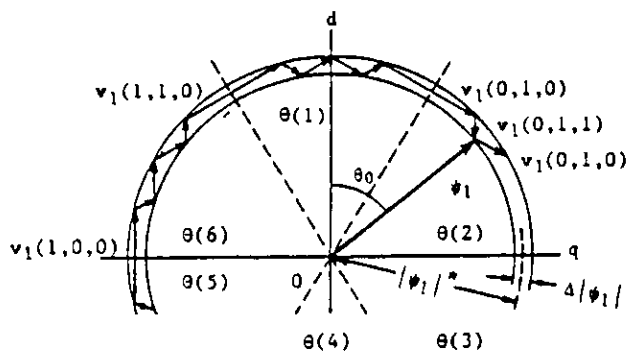

Fig.5. Selection of voltage vectors for ψ_1

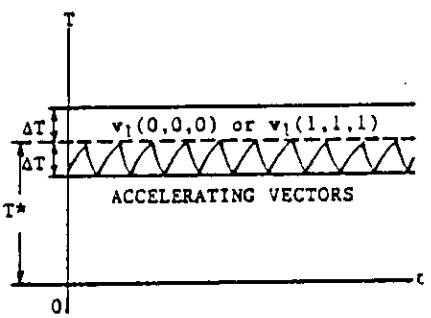

Fig.6. Selection of voltage vectors for T

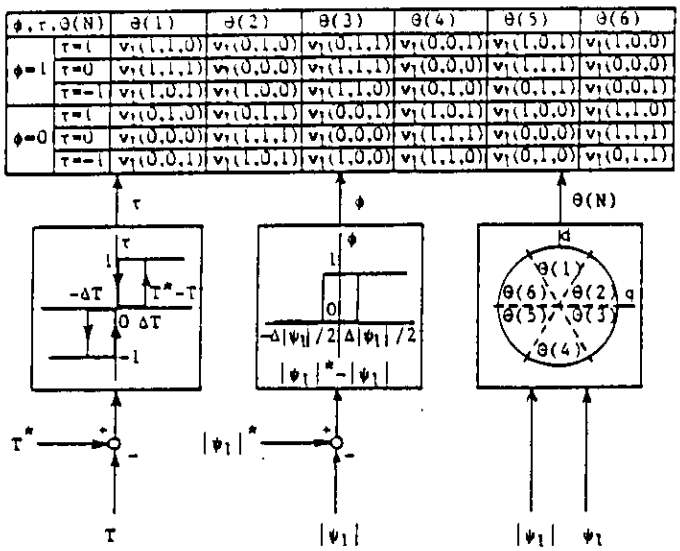

Fig.7. Optimum switching table and comparators

V. FLUX CONTROL FOR EFFICIENCY IMPROVEMENT

Torque control is skillfully obtained by controlling the instantaneous slip angular frequency, whereas the improvement of the efficiency can be achieved by controlling the amplitude of ψ_1 like a field weakening operation. In the case of frequent changes of the torque command, it is necessary to keep the amplitude of maximum. Under the field weakened state, the sufficient torque or quick torque response would not be expected because of the slow response of the flux increase. On the other hand, in the steady state operation, especially at light loads, the maximum efficiency can be obtained at a low flux level. Therefore, in oder to obtain the muximum efficiency, the flux level is adjusted automatically in accordance with the torque command.

Fig.8 shows a block diagram of the efficiency controller. A nonlinear active filter is composed of an integrator with a diode. It behaves like a peak holder when the torque command T* changes frequently. The integrator output voltage increases as fast as possible because of the small charging time constant. When once the voltage settles to a certain value, it decreases very slowly because the discharging time constant is very large. These time constants are specified appropriately according to the frequence of the torque command change. The nonlinear function element is employed to determine the flux command so as to achieve the maximum efficiency in the steady state operation. The function is approximated as square root one except for the magnetic saturation of the motor.

The total loss of the induction motor is expressed by

$$P\,loss = R_1 I_1^2 + R_2' I_2'^2 + Ri I_0^2 \tag{19}$$

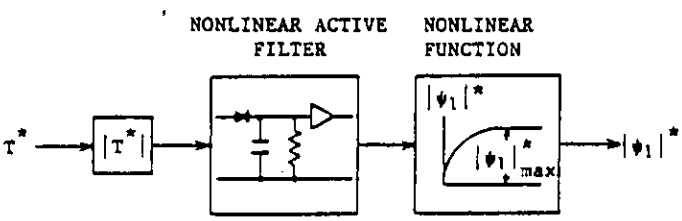

Fig.8. Block diagram of efficiency controller

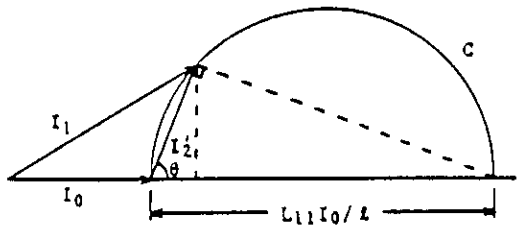

Fig.9. Circular diagram

where R_2' : R_2 referred to the stator, Ri : equivalent resistance of the iron loss, I_1, I_2' : rms values of I_1 and I_2 referred to the stator respectively. The equation can be rewritten with respect to I_2' and I_0 as

$$P\,loss = (R_1+R_2')I_2'^2 + (R_1+Ri)I_0^2 + 2R_1 I_0 I_2' \cos\theta \tag{20}$$

where the trajectory of I_2' is on the circle C as shown in Fig.9. θ is the phase difference between I_0 and I_2'. The electromagnetic torque of Eq.(10) can be also rewritten using θ.

$$T = L_{11} I_0 I_2' \sin\theta \tag{21}$$

Since the voltage across the leakage reactance, $\omega(L_{11}/M)^2 \ell I_2'$, is equal to $\omega L_{11} I_0 \cos\theta$, therefore, the following relation can be obtained.

$$I_2' = \frac{L_{11}}{(L_{11}/M)^2 \ell} I_0 \cos\theta \tag{22}$$

Substituting Eq.(22) into Eqs.(20) and (21) gives

$$P\,loss = \frac{2(L_{11}/M)^2 \ell T}{L_{11}^2} \left(\frac{A\cos^2\theta + B}{\sin 2\theta}\right) \tag{23}$$

where

$$A = \frac{L_{11}}{(L_{11}/M)^2 \ell}\left[L_{11}(R_1+R_2')/(L_{11}/M)^2 \ell + 2R_1\right]$$

$$B = R_1 + Ri$$

The total loss of Eq.(23) has the minimum value at $\theta = \tan^{-1}\sqrt{(A+B)/B}$. Substituting $\theta = \tan^{-1}\sqrt{(A+B)/B}$ into Eq.(21) and (22), the solution is derived as follows.

$$T = \frac{1}{(L_{11}/M)^2 \ell}\,\frac{\sqrt{AB+B^2}}{A+2B}\,|\psi_1|^2 \tag{24}$$

Therefore, the optimum flux linkage is propotional to the square root of the electromagnetic torque.

VI. EXPERIMENTAL SYSTEM AND RESULTS

Fig.10 shows a configuration of the proposed system. In this system, the d and q-axis variables are used for convenience instead of the instantanous vectors. So the three-to-two phase transformations for the primary voltage and current are given by

$$\begin{aligned} v_1 &= v_{1d} + j v_{1q} \\ &= \sqrt{2/3}\left[v_{1a} - v_{1b}/2 - v_{1c}/2 + j(\sqrt{3}v_{1b}/2 - \sqrt{3}v_{1c}/2)\right] \\ i_1 &= i_{1d} + j i_{1q} \\ &= \sqrt{2/3}\left[i_{1a} - i_{1b}/2 - i_{1c}/2 + j(\sqrt{3}i_{1b}/2 - \sqrt{3}i_{1c}/2)\right] \end{aligned} \tag{25}$$

Substituting Eq.(25) into Eq.(14), the components of the primary flux linkage vector are expressed as

$$\begin{aligned} \psi_1 &= \psi_{1d} + j\psi_{1q} \\ &= \int(v_{1d} - R_1 i_{1d})dt + j\int(v_{1q} - R_1 i_{1q})dt \end{aligned} \tag{26}$$

The d and q-axis components of ψ_1 can easily calculated by using integrators as shown in above equation. The electromagnetic torque in Eq.(5) is rewritten as

$$T=\psi_{1d}i_{1q}-\psi_{1q}i_{1d} \tag{27}$$

The equation shows that the torque can be estimated by only the primary variables. Then the errors of the amplitude of the flux and torque need to be digitalized by two and three level hysteresis comparators respectively, and digitalized direction of ψ_1, $\theta(N)$, is determined by comparing ψ_{1d} and ψ_{1q} with $\pm\sqrt{3}/2|\psi_1|$ or $\pm 1/2|\psi_1|$ using some comparators and logic circuits. The optimum switching table is referred by the digital signals, i.e. one bit of ϕ, two bits of τ and three bits of $\theta(N)$. Thus the optimum voltage vector $v_1(Sa,Sb,Sc)$ can be obtained directly by accessing the address of the ROM of which memory size is only 64 bytes. If an A/D converter were employed instead of the comparators, the more excellent performance and precise control would be expected. The outputs of the ROM are directly used to drive the power transistors after isolated by photo couplers.

The control circuit can be simplified because the scheme needs neither the secondary variables and constants of the machine nor the coordinate transformation using a position sensor, whereas integrators cause some drift and operation errors at low velocity regions. But the effect is very small above 2 Hz, so the compensation for flux calculation is not always necessary at normal operation. For extremely low velocity operation, another estimation of the flux may be necessary as stated later.

Experiments were carried out to verify the feasibility of the proposed scheme using a 1.5 kW three phase induction motor. Fig.11(a) shows a locus of the primary flux linkage in the steady state. $|\psi_1|$ is controlled to be approximately constant and several bright spots show the points where ψ_1 halts. Since flux ripple are relatively small and minorloops are not observed in this locus, harmonic losses and acoustic noise of the machine may be effectively decreased [9] . Fig.11(b) shows a velocity step response obtained in the experiment. The response time for the velocity difference of 500 rpm is about 8 msec. Even in the transient operation, $|\psi_1|$ can be kept constant owing to the limit cycle control except for saturation of the inverter. The harmonic components of the electromagnetic torque are also restricted within the hysteresis bands. The switching frequency of the comparators is identical with that of the PWM inverter. Hence, using proposed control, the inverter switching frequency can be reduced under the same condition of torque and flux ripple in comparison with the other schemes. Since the ripples have relation closely to the acoustic noise and harmonic losses, the proposed scheme will make possible decreasing not only the inverter switching frequency but also the else harmful components. Fig.12(a) and (b) show the improved results of the efficiency and acoustic noise, respectively, by using the efficiency controller. When the amplitude of ψ_1 is 33 % of the maximum value, no load loss can be improved less than 70 W and the acoustic noise level is also decreased by 10 - 15 dB.

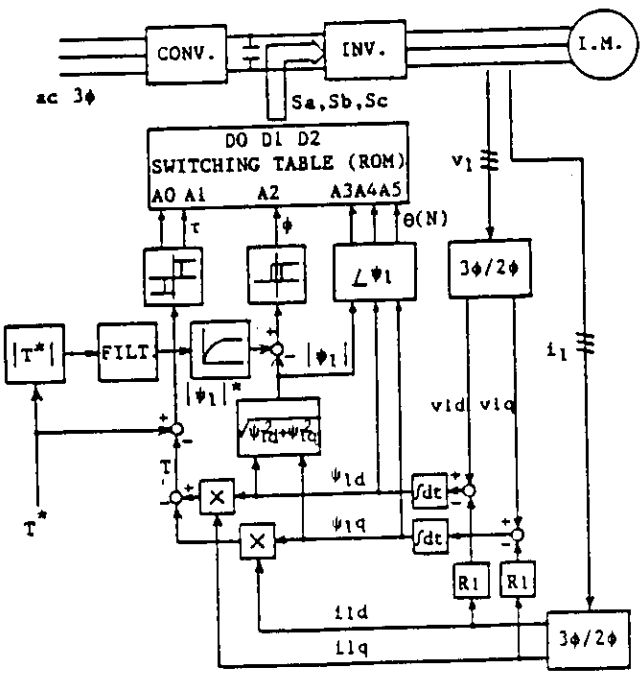

Fig.10. Block diagram of proposed system

Fig.11.
Experimental results
(a) Locus of ψ_1 at 600 rpm
(b) Velocity step response

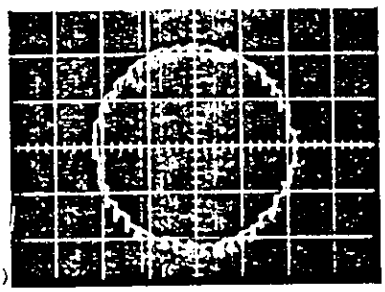

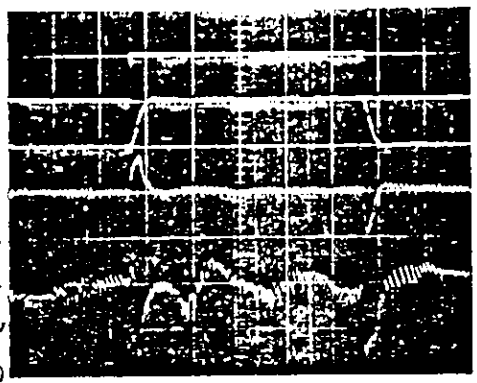

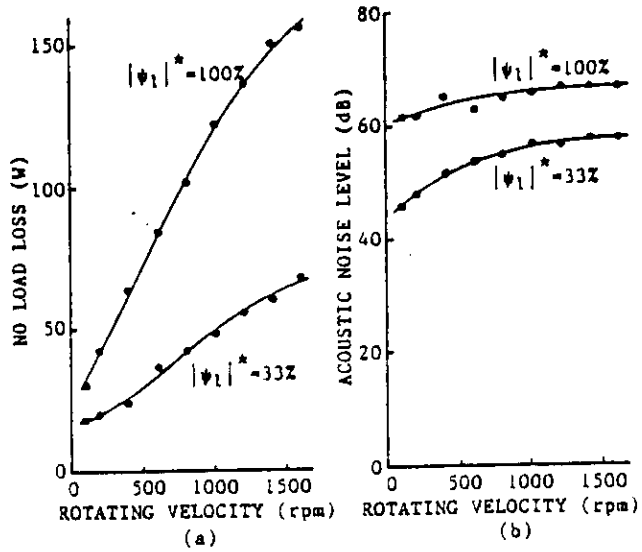

Fig.12. Efficiency improvement and noise reduction
(a) No load loss, (b) Acoustic noise level

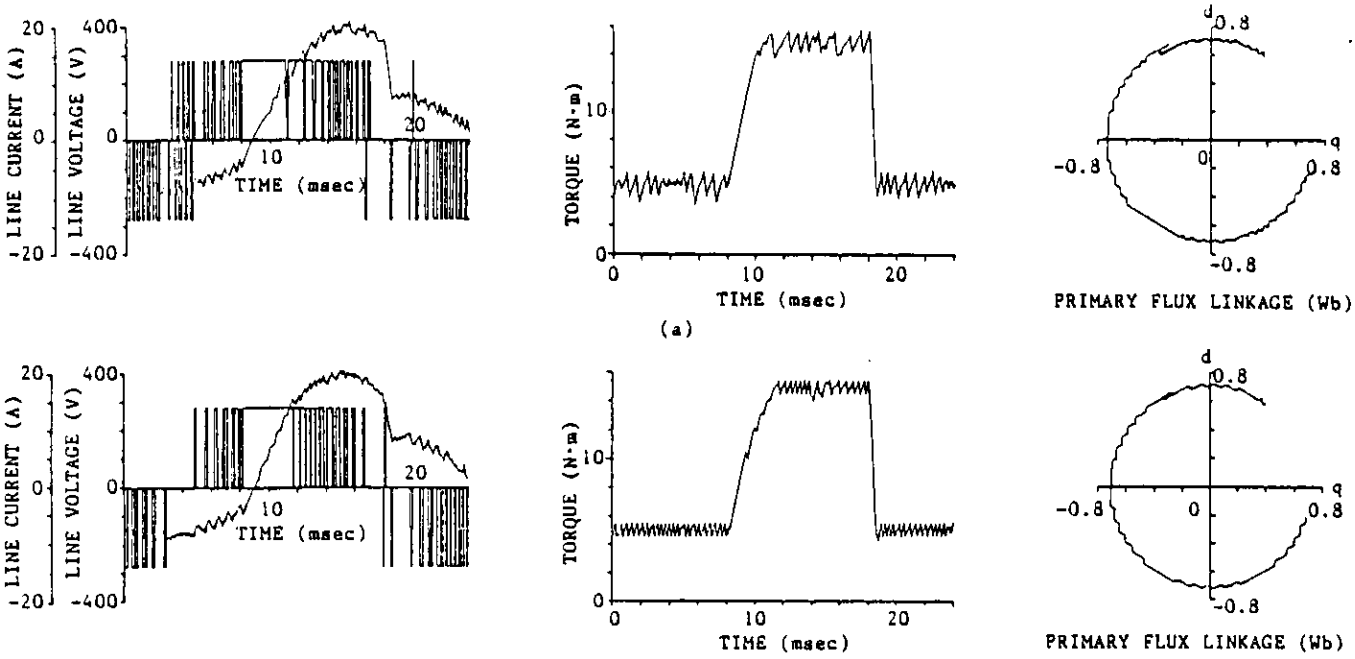

Fig.13. Simulation results for comparison between two schemes
(a) Field oriented control
(b) Proposed control

Induction motor parameters;
R_1 : 0.5 Ω, R_2 : 1.0 Ω
L_{11} : 0.105 H, L_{22} : 0.105 H
M : 1.0 H, Number of poles : 2
$\dot{\theta}m$: 188.5 rad/sec (1800 rpm)
V : 280 V, Switching frequency : 2.5 kHz

VII. COMPARISON WITH FIELD ORIENTED CONTROL

Assuming field oriented control employing an instantaneous current controlled inverter by hysteresis comparators and the same inverter switching frequency and dc link voltage, the comparison between field oriented and proposed control is performed.

Fig.13(a) and (b) show simulation results of the torque step responses from 5 N·m to 15 N·m. As shown in this figure, the flux ripples of both schemes are almost same, whereas the torque ripple of this scheme is about half of conventional one in the steady state.

It has been said that the field oriented controller can achieve the torque response instantaneously. But this can be said only when the inverter can achieve instantaneous current control sufficiently. In other words, when the inverter output voltage is limited, the instantaneous response would not be assured. In the proposed system, the optimum voltage vector can be selected to obtain as fast torque response as possible at every instant. Therefore, the response when the inverter saturates bears comparison with that of field oriented control. Moreover, owing to the effective switching operation, the reduction of the inverter switching frequency is remarkable especially in the low velocity operation.

Eq.(12) represents the effect of the rotor resistance variations on the response, which clearly shows that the increase of R_2 causes deterioration of the response. Fig.14 shows that the small deterioration of the response time is observed as R_2 increases. In the practical case, however, the deviations of R_2 from 50% to 150% would scarecely cause the serious problems. Thus torque limit cycle control employed in this scheme is very effective for designing a robust system. On the other hand, the deviations of the stator resistanse R_1 causes some errors in calculating

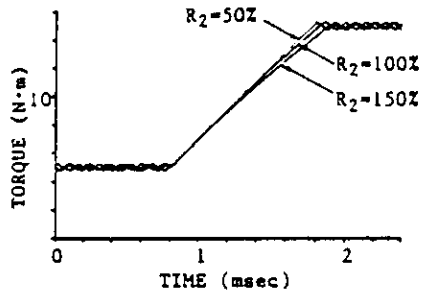

Fig.14. Torque step response for variations of R_2

ψ_1 using Eq.(14) at low velocities. Therefore, a compensator for the flux calculation is necessary to be implemented.

VIII. COMPENSATION FOR FLUX CALCULATION

Eq.(14) indicates that the primary flux linkage vector ψ_1 can be calculated from only the primary variables, which are observable and measured with simple circuits. Some problems, however, would arise from the integral operation at extremely low velocities. The reason of this is that the operation of integrators can not be perfectly done at zero velocity because of no induced electromotive force in the motor, so that control of ψ_1 might be unstable when R_1 deviates from the correct value. These problems are negligible at relatively high velocities such as above 2 Hz. But another calculation of ψ_1 must be employed below 2 Hz.

Transforming Eq.(4) with respect to an α-β frame synclonously roatating with the rotor, then the result can be written as

$$\begin{bmatrix} v_1' \\ 0 \end{bmatrix} = \begin{bmatrix} R_1+(p+j\dot{\theta}m)L_{11} & (p+j\dot{\theta}m)M \\ pM & R_2+pL_{22} \end{bmatrix} \begin{bmatrix} i_1' \\ i_2' \end{bmatrix} \quad (28)$$

And the flux linkage vector in the α-β frame is

$$\psi_1' = L_{11}i_1' + Mi_2' \quad (29)$$

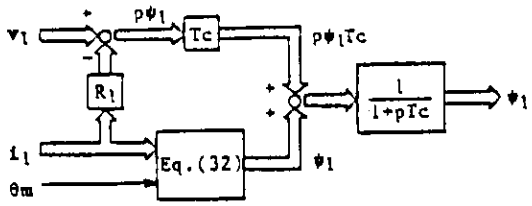

Fig.15. Improved flux estimator

Substituting i_2' from the rotor equation into Eq.(29), ψ_1' can be rewritten with respect to i_1' as follows.

$$\psi_1' = L_{11}\frac{1+p(\ell/R_2)}{1+p(L_{22}/R_2)}i_1' \qquad (30)$$

Equations describing the coordinate transformation are given below.

$$\psi_1 = \psi_1'\exp(\mp j\theta m),\quad i_1' = i_1\exp(j\theta m) \qquad (31)$$

Then, substituting Eq.(31) into Eq.(30) gives

$$\psi_1 = \left(L_{11}\frac{1+p(\ell/R_2)}{1+p(L_{22}/R_2)}[i_1\exp(j\theta m)]\right)\exp(-j\theta m) \qquad (32)$$

Hence, ψ_1 can be calculated from i_1 and θm even at low velocities, but variations of R_2 affects this calculation [6].

Accordingly, in order to calculate the flux precisely, it is better to employ Eq.(14) than Eq.(32) at relatively high velocities. At low velocities such as below 2 Hz, Eq.(32) is better to the contrary. Fig.15 shows an improved flux estimator circuit composed of a simple lag network. The input of the network is $Tcp\psi_1+\psi_1$, therefore, the output is equal to ψ_1. In this figure, the time constant Tc must be specified so as to minimize automatically the calculation error when the flux equation changes from Eq.(14) to Eq.(32). In the case of the low velocity operation, i.e. $\omega Tc<<1$, the network behaves as a circuit of unity transfer function. Thus its output becomes almost ψ_1 of Eq.(32) because of the small value of $v_1-R_1i_1$ in Eq.(14). In the high velocity operation, since $1<<\omega Tc$, the transfer function is approximately shown as $1/s$, which corresponds to that of the integrator. Hence, these actions are switched over smoothly around the frequency of $1/Tc$.

Fig.16(a) shows the trajectory of ψ_1 at 1 rpm when the stator resistance varied by +20 %. The trajectory is shifted and, as a result, ψ_1 would be saturated. Whereas, Fig.16(b) shows the compensated result using above scheme. As can be seen from this figure, the shifting is fully compensated.

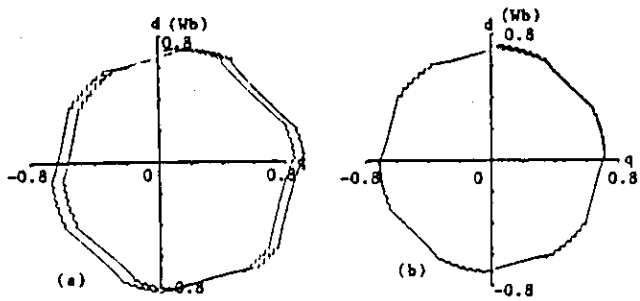

Fig.16. Trajectory of ψ_1
(a) In the case of $R_1'=1.2R_1$
(b) Compensated result

IX. CONCLUSION

Novel induction motor control optimized both torque response and efficiency is proposed. The control is quite different from usual field oriented control because it depends on the concept of the instantaneous slip frequency control in spite of the electromagnetic force. In another words, the former is to "Arago's law" as the latter is to "Fleming's law".

Through the experimental and simulation technique, validity of the proposed theory can be made to clarify. The main results obtained in this paper are as follows;

(1) In the transient state, the highest torque response can be obtained by selecting the fastest accelerating voltage vector to produce the maxmum slip frequency.

(2) In steady state, by selecting the accelerating vector and the zero voltage vector alternately, the torque can be maintained constant with small switching frequency by the hysteresis comparator of torque. Accordingly, the harmonic losses and the acoustic noise level of the motor can be reduced.

(3) The amplitude of the primary flux is also controlled in order to attain the maximum efficiency in the steady state operation. The flux level can be automatically adjusted to get the optimum efficiency in the steady state and the highest torque response in the transient state at the same time by using a nonlinear active filter.

(4) At extremely low frequency operation, the proposed control circuit makes some drift, but it can be easily compensated automatically to minimize the effect of the variation of the machine constants.

The proposed scheme is found to be very promising and valuable corresponding to the field oriented control. All of the results show that the scheme is superior in every respect to the field oriented control.

ACKNOLEDGEMENTS

The authors wish to express their appreciation to the Power Electronics Laboratory members and Mr.Y. Ohmori of Technological University of Nagaoka. Also the financial support by the Heavy Apparatus Standard Products Department of Toshiba Corporation is gratefully acknowledged.

REFERENCES

[1] A. Nabae, K. Otsuka, H. Uchino and R. Kurosawa, "An approach to flux control of induction motors operated with variable-frequency power supply," IEEE Trans. Ind. Appl., vol. IA-16, pp. 342-350, May/Jun. 1980.

[2] L. J. Garces, "Parameter adaption for the speed controlled static ac drive with a squirrel-cage induction motor," IEEE Trans. Ind. Appl., vol. IA-16, pp. 173-178, Mar./Apr. 1980.

[3] K. B. Nordin, D. W. Novotny and D. S. Zinger, "The influence of motor parameter deviations in feedforward field orientation drive systems," in Conf. Rec. 1984 Annu. Meet. IEEE Ind.Appl. Soc., pp. 525-531.

[4] T. Matsuo and T. A. Lipo, "A rotor parameter identification scheme for vector controlled induction motor drives," in Conf. Rec. 1984 Annu. Meet. IEEE Ind. Appl. Soc., pp. 538-545.

[5] T. Noguchi and I. Takahashi, "Quick torque response control of an induction motor based on a new concept," IEEJ Tech. Meet. on Rotating machine RM84-76, pp61-70, Sep. 1984.

[6] I. Racz, "Dynamic behaviour of inverter controlled induction motors," in Conf. Rec. 1965 IFAC, pp. 48.1-48.7.

[7] K. R. Jardan, S. B. Dewan and G. R. Slemon, "General analysis of three-phase inverters," IEEE Trans. Ind. Gen. Appl., vol. IGA-5, pp. 672-679, Nov./Dec. 1969.

[8] K. R. Jardan, "Modes of operation of three-phase inverters," IEEE Trans. Ind. Gen. Appl., vol. IGA-5, pp. 680-685, Nov./Dec. 1969.

[9] Y. Murai and Y. Tsunehiro, "Improved PWM method for induction motor drive inverters," in Conf. Rec. 1983 IPEC, pp. 407-417.